Bulletin of Earthquake Engineering
https://doi.org/10.1007/s10518-019-00758-2

ORIGINAL RESEARCH

Simplified seismic assessment of infilled RC frame structures

Al Mouayed Bellah Nafeh[1] · **Gerard J. O'Reilly**[2] · **Ricardo Monteiro**[2]

Received: 7 March 2019 / Accepted: 22 November 2019

Abstract
Earthquake-induced structural damage, characterised by the exceedance of different damage states during ground shaking, is typically quantified using fragility curves generated through non-linear dynamic analyses often requiring a large computational effort. This level of effort has led to the necessity of simplified methods and approximate analysis tools. In this regard, SPO2IDA has emerged as a convenient tool for the assessment of structures. It relates a structure's backbone characteristics to a set of incremental dynamic analysis (IDA) curves using static pushover analysis (SPO) results and a library of empirical fitting coefficients for the different branches of the idealised SPO backbone. It permits the quantification of structural performance up to structural collapse as a function of seismic intensity in a simple and efficient manner. It has been developed mainly for ductile structures that can be sufficiently represented via a SPO backbone with a certain ductile post-yield hardening followed by a post-peak degradation. This behaviour is quite representative of ductile RC and steel moment-resisting frames and has resulted in the tool being widely adopted. However, the same may not be observed when dealing with reinforced concrete (RC) frames with masonry infill, a structural typology that still requires significant addressing in the earthquake engineering field. The present study describes an extension to this methodology for structural typologies with a more particular backbone behaviour, typical of RC frames with masonry infill panels, since differences in backbone behaviour compared to typical structures render the extension of the original tool inappropriate and at times unconservative. Extensive analyses were conducted to investigate the behaviour and trends when pushing infilled RC frames up to complete structural collapse. A new library of empirical coefficients was then fitted and proposed by considering a large database of representative backbones to result in an extended SPO2IDA proposal for infilled RC frames. It is then shown how these coefficients provide a much-improved matching, when compared to the original tool for this specific case, both in terms of the produced IDA traces and also the drift-based mean annual rates of exceedance.

✉ Gerard J. O'Reilly
gerard.oreilly@iusspavia.it

Al Mouayed Bellah Nafeh
mouayed.nafeh@iusspavia.it

Ricardo Monteiro
ricardo.monteiro@iusspavia.it

[1] Università degli Studi di Pavia, Pavia, Italy

[2] Scuola Universitaria Superiore IUSS Pavia, Pavia, Italy

Published online: 02 December 2019

Keywords Seismic assessment · Collapse · Seismic risk · Infilled frames · SPO2IDA

1 Introduction

Assessing the structural performance of existing reinforce concrete (RC) frame buildings designed prior to the introduction of modern seismic design provisions around the 1970s typically involves an analysis of serviceability limit states, collapse performance and the behaviour of the structure itself conditioned on non-global collapse. As such, the ability to accurately quantify the exceedance of any structural demand-based performance level is of great interest and is typically quantified with fragility curves, where the exceedance probability of a certain performance limit state can be expressed as a function of seismic shaking intensity. These are usually the end-result of extensive numerical modelling, ground-motion selection, non-linear dynamic analyses and post-processing of the subsequent results, which typically require large computational effort and time depending on the complexity of the numerical modelling and the extent of the analysis procedure adopted. To somewhat reduce this computational burden, a number of simplified tools and methodologies for the assessment of RC frame structures have emerged in the literature over the past number of years, with the introduction of the SPO2IDA tool (Vamvatsikos and Cornell 2005) being a notable example. It empirically relates the static pushover (SPO) curve to its corresponding incremental dynamic analysis (IDA) traces (Vamvatsikos and Cornell 2002) and permits the characterisation of the structural performance in a simplified manner. A recent extension of this simplified procedure, SPO2FRAG (Baltzopoulos et al. 2017), related the SPO curve directly to the fragility curves of specific limit states, in addition to other considerations. The main scope behind such tools is to aid the quantification and mitigation of seismic risk with respect to different guidelines and procedures (FEMA 2000, 2005, 2009; Pinto and Franchin 2014; CNR 2014) and supply users with means with which to reduce computational effort and processing time. The inclusion of SPO2IDA as a simplified tool in the FEMA P-58 guidelines (FEMA 2012), for example, attested to the value of this kind of simplified tools in performance-based earthquake engineering (Cornell and Krawinkler 2000).

These simplified tools employ what are typically referred to as R–μ–T relationships, developed through extensive dynamic analyses, that empirically relate the strength reduction factor, R, of a single degree of freedom (SDOF) oscillator to the elastic spectral demand of a ground motion to its period of vibration, T, and subsequent ductility demand, μ. These R–μ–T relationships were previously quantified for given SPO backbone curves typologies and implemented in the background of the tools themselves. The end result of this is to convert the SPO curve parameters of a multi-degree of freedom (MDOF) system (e.g. base shear, V_b and roof displacement, Δ) into an equivalent SDOF (i.e. force, F^* and displacement, Δ^*) and then quantify the IDA traces, or the fragility curves directly, using these empirical relationships.

The recent work by O'Reilly and Sullivan (2018) has shown that these existing tools may not be entirely adequate for the characterisation of infilled RC frame typologies since the available empirical R–μ–T relationships were not established to represent such SPO backbone characteristics (i.e. high initial stiffness and strength followed by sudden loss of strength and stiffness upon infill panel collapse) as it was mainly targeting other structural configurations, such as ductile moment frames designed with modern design code provisions. This idea that existing RC frames with masonry infill panels cannot be reasonable

represented by a simple bilinear hysteretic backbone has existed for some time and studies such as the ones by Dolšek and Fajfar (2004, 2005) were among the first to thoroughly address this issue, both from a numerical modelling perspective and also a simplified implementation viewpoint.

Keeping the above remarks in mind, regarding the simplified assessment of RC frames with masonry infill, some further extension is required. This relates to both the simplified assessment via SDOF oscillators all the way to structural collapse, in addition to the simplified assessment via SPO2IDA-oriented tools. For this reason, an exhaustive campaign was performed in this study in an effort to establish new R–μ–T relationships through assessment of numerous infilled RC frames typologies. A library of empirical coefficients was quantified, essentially providing an extension for the original SPO2IDA tool to this specific structural typology. The emphasis of this study was to permit the adequate assessment of these structural typologies in an efficient and simplified manner within the already established guidelines and procedures available and implemented for other structural typologies.

2 Assessment of infilled RC frames with equivalent SDOF oscillators

2.1 Description and numerical modelling of case study structures

A total of five case study structures with varying number of storeys (2, 3, 4, 6 and 9) and infill typology [i.e. 'weak' and 'strong' as per Hak et al. (2012)] were adopted from a previous study by O'Reilly and Sullivan (2018). These structures may be considered representative of infilled RC frames constructed in Italy prior to the introduction of modern seismic design provisions in the 1970s. They were designed to resist gravity loading only and did not consider capacity design principles, which constitute a crucial aspect of modern seismic design. The presence of masonry infill on the overall lateral response of the structure was also not considered, which was quite common throughout Italy and the rest of the Southern Mediterranean at that time.

Numerical modelling of these case study structures and subsequent analyses were conducted using OpenSees (McKenna et al. 2010) and the techniques used to model these structures are described in O'Reilly and Sullivan (2017). This modelling approach was calibrated to available experimental data that accounts for the strength and stiffness degradation of the frame members, the effects of smooth reinforcing bars with end-hooks, in addition to the strength and stiffness degradation in the beam–column joints. The effects of the presence of masonry infill on the global structural response was incorporated using the equivalent diagonal strut approach described by Crisafulli and Carr (2007). The first mode periods of these structures are listed in Table 1.

SPO analyses were conducted for each structure, using a displacement-controlled lateral load pattern proportional to its first mode shape. Figure 1 shows the SPO curves where

Table 1 First mode periods of vibration, T_1, for each case study structure

Typology	2 Storey	3 Storey	4 Storey	6 Storey	9 Storey
Bare frame	0.85	1.22	1.52	1.97	2.72
Infilled frame (weak infill)	0.25	0.37	0.44	0.63	1.00
Infilled frame (strong infill)	0.15	0.21	0.29	0.41	0.65

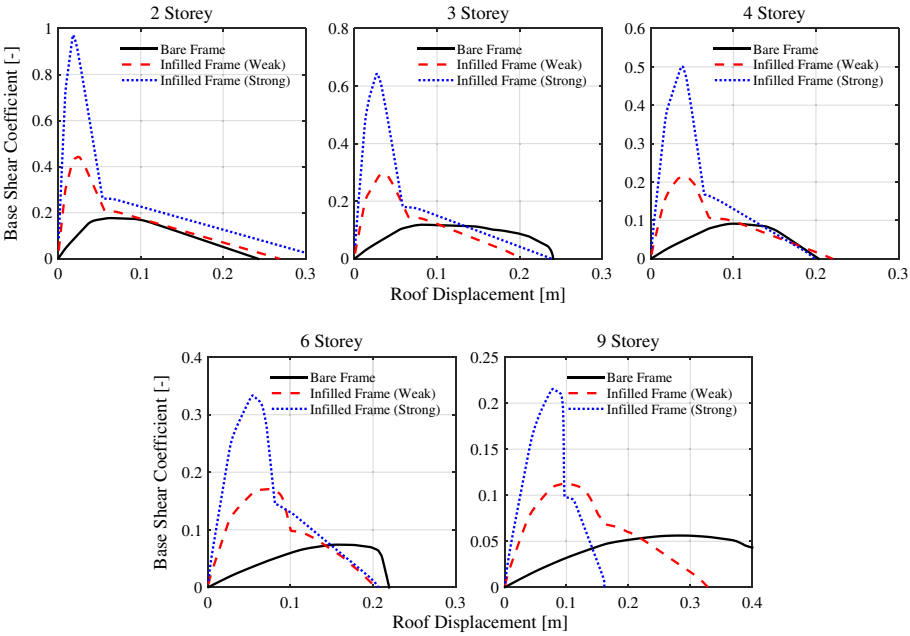

Fig. 1 Static pushover curves showing base shear coefficient versus roof displacement of the case study structures, where the influence of masonry infill presence and typology on the lateral strength is evident

the base shear coefficient—defined as the base shear, V_b, normalised by the total building weight, W—is plotted against the roof displacement, Δ, for three different variations of the case study structures. These correspond to: 'bare frame', where no infill was present in the numerical model; 'strong infill', where a uniform distribution of the corresponding infill typology outlined in Hak et al. (2012) was considered; and 'weak infill', where a uniform distribution of that infill typology (Hak et al. 2012) was considered. As clearly illustrated in Fig. 1, the presence of masonry infills considerably modifies the lateral behaviour compared to the bare frames, noticeable through the increase in initial stiffness, peak lateral strength and sudden drop in lateral load-bearing capacity. Moreover, the effect of the infilled frames' soft-storey mechanism is noticeable through their post-peak behaviour, sometimes exhibiting a lower displacement capacity and quicker reduction in lateral capacity when compared to bare frames. This may be attributed to the concentration of damage at a single storey in the infilled frames, as opposed to a more distributed deformation in bare frames, meaning that global flexibility is reduced and damage is accumulated faster, resulting in a more accelerated reduction in lateral strength.

2.2 Equivalent SDOF conversion and numerical modelling

The previous section discussed the characterisation of infilled RC frames via SPO analysis using numerical models that consider the individual structural element characteristics in a direct manner. This is generally the preferred option when analysing structural behaviour in a static analysis context. However, when moving to the more computationally expensive dynamic analysis with numerous ground motion records, the use of a more simplified

structural representation via equivalent SDOF models may be a more convenient option. This is to capture key structural characteristics whilst permitting robust analyses in a quick and efficient manner. Examples of contexts that favour such an approach are present in simplified assessment methods like the pushover-based assessment method proposed by Fajfar and Dolšek (2012) or in more regional-oriented approaches such as that outlined in Villar-Vega et al. (2017).

In the context of infilled RC frames, this topic has received relatively little specific attention compared to other more prominent typologies. For example, D'Ayala et al. (2015) published guidelines on how SDOF models (Villar-Vega et al. 2017) may be developed for typologies including infilled RC frames. Figure 2a illustrates this generic backbone definition, adopted also in Villar-Vega et al. (2017) and herein referred to as 'Approach 1', whereby the general shape of the SPO curve resembles those illustrated in Fig. 1 for strong infills, with a large strength and stiffness followed by a drop in lateral strength due to the failure of the masonry infill panels. This backbone is established using the results of a simple SPO analysis or by assuming some typical lateral capacity ranges. It is then converted to an equivalent SDOF via standard structural dynamics manipulations assuming a first-mode-dominant response. An ultimate displacement of the equivalent system is typically defined and the backbone response is assumed to follow the fixed shape illustrated in Fig. 2a. That is, no specific treatment is given to the fact that following the first cycle that breaks the masonry infill at the critical storey, the lateral resistance and stiffness will be greatly reduced for all subsequent cycles. This change in lateral stiffness and subsequently the first-mode period of vibration has a number of impacts on the efficiency of different intensity measures (O'Reilly et al. 2018a) or to the expected level of dispersion for different demands parameters of interest (O'Reilly and Sullivan 2018). One study that acknowledged this characteristic behaviour and incorporated it into a simplified model was the one by Dolšek and Fajfar (2004), whereby the initial strength and stiffness contribution of the masonry infill was incorporated separately alongside another model to represent the underlying RC frame to give a generic backbone shape as outlined in Fig. 2b, which is herein referred to as 'Approach 2'. While the establishment of these backbone parameters was not specifically addressed by Dolšek and Fajfar (2004), an important development was by considering the contributions of the RC frame and masonry infill separately, unlike the model illustrated in Fig. 2a. Of particular importance for the model in Fig. 2b is that

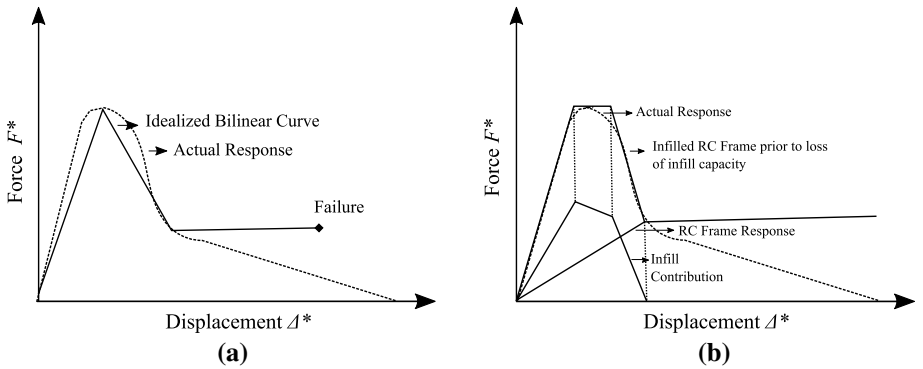

Fig. 2 Illustration of **a** Approach 1 utilised in past studies such as Villar-Vega et al. (2017), **b** Approach 2 developed by Dolšek and Fajfar (2004) for infilled RC frames

unlimited ductility was assumed for the RC frame and no strength nor stiffness degradation was foreseen.

The two modelling strategies for equivalent SDOF systems illustrated in Fig. 2 represent reasonable approaches to capture the overall behaviour of infilled RC frames. However, some particular aspects may still be improved to better represent the physical reality of what is happening during lateral response. For example, considering a defined ultimate displacement capacity of these structures is of undoubted importance when examining behaviour up to collapse. To such extent, Approach 1 is more favourable since Approach 2 assumes infinite ductility of the underlying RC frame. On the other hand, what is favourable about Approach 2 is the way in which it segregates the masonry infill contribution from the RC frame contribution. However, this approach also requires further attention because while the overall backbone of the infilled RC frame ought to resemble that found from a simple SPO analysis (e.g. Fig. 1), the subsequent response of the structure following the collapse of the masonry infill at the critical storey in the building does not exactly become the response of a completely bare frame. In the case of older RC frames with masonry infill, the infill collapse tends to occur at a single storey meaning that the subsequent response will be more of a soft-storey response in the critical storey, but with significant stiffness remaining at the other non-critical storeys. Therefore, the response of the underlying RC frame illustrated in Fig. 2b should be that of the infilled RC frame with the critical storey's masonry infill removed and not of the completely bare frame, as illustrated in Fig. 3. This way, the effect of losing the masonry at the critical storey is modelled in a more similar manner to the real behaviour. It must be stated that Dolšek and Fajfar (2004) did not actually delve into the details of how to establish the parameters of the model illustrated in Fig. 2b and it may also be interpreted as described above. O'Reilly et al. (2018a) discussed this aspect briefly for the structures examined here where the modal properties of the infilled RC frame's numerical model with the critical storey's infill removed showed a significant increase in the first mode period, but was still notably lower than that of the structure modelled without any masonry infill. An important aspect to note is that only the in-plane response of the masonry infill panels is considered in this study and full contact between the infill panels and the surrounding frame is assumed. The influence of in-plane/out-of-plane interaction is not taken into account due to the simplified nature of the proposed tool. Interested readers are referred to other studies (Ricci et al. 2018; Furtado et al. 2016; Pasca et al. 2017) for further details on this topic.

Considering the above remarks, a more refined equivalent SDOF modelling approach for infilled frames is proposed herein. It essentially combines the two approaches discussed previously to permit a more representative characterisation of an infilled RC frame's behaviour up to collapse. It comprises a 'crackable' backbone similar to

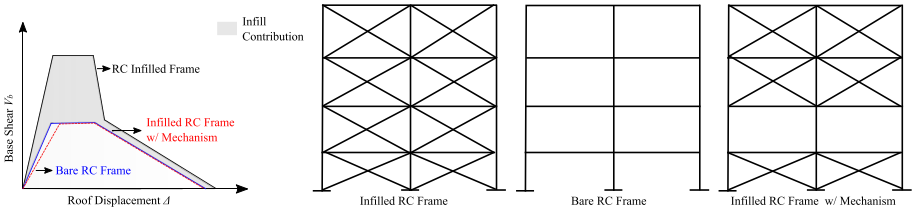

Fig. 3 Differences in SPO curves between bare frame, completely infilled RC frame and infilled RC frame with mechanism formed at the critical storey, where the significant difference in the initial stiffness between the bare RC frame and infilled RC frame with the critical storey's infill panels removed is noted

Approach 2 described previously, but also a more representative ultimate behaviour whereby the strength and stiffness degradation of the underlying RC frame is also captured, instead of assuming unlimited ductility or constant strength to a predetermined ultimate displacement, as in Approach 1. Figure 4 outlines the basics of this model, where the SPO backbone of the two models is required. First, examining the results of the infilled RC frame's response, the backbone parameters (i.e. points 0–1–2–3–4) can be found. By examining the evolution of the displaced shape, the location of the critical storey can be identified from this first SPO analysis. By removing the infill struts in the numerical model at this storey and repeating the SPO analysis, the backbone parameters for the RC frame with mechanism (i.e. points 0–5–6–7) can be identified. The soft-storey mechanism is assumed to occur after the sudden degradation in strength. Thus, the residual plateau is defined as the shift from infilled frame to the frame with induced soft-storey. The aim behind modelling both behaviours separately is to increase the robustness of the numerical model through the inclusion of period-elongation effect when transitioning between stiffnesses and thus realistically mimicking the hysteretic behaviour.

To implement this equivalent SDOF model in addition to the others described in Fig. 2, the results of the SPO analysis of the MDOF structures illustrated in Fig. 1 are taken and transformed to their equivalent SDOF counterparts. By taking the base shear, V_b, and roof displacement, Δ, values from each model, the SDOF transformations are characterised by their force, F^*, and displacement, Δ^*, values and effective mass, m^*, all of which are computed as follows:

$$F^* = \frac{V_b}{\Gamma} \tag{1}$$

$$\Delta^* = \frac{\Delta}{\Gamma} \tag{2}$$

$$m^* = \sum_i m_i \Phi_i \tag{3}$$

where Γ represents the first mode transformation factor computed as:

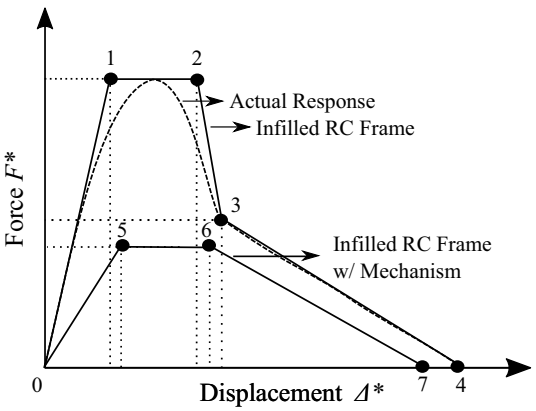

Fig. 4 Illustration of the proposed modelling strategy where the actual response of the infilled RC frame (i.e. 0–1–2–3–4) is shown with the structural response once the critical storey has formed a mechanism and its masonry infill panels have collapsed (i.e. 0–5–6–7). Thus, the proposed model comprises a combination of this latter model and the infill contribution to give the 0–1–2–3–4 response initially but reduces to the 0–5–6–7 response once the infill has collapsed

$$\Gamma = \frac{m^*}{\sum_i m_i \Phi_i^2} \tag{4}$$

The terms m_i and ϕ_i represent the mass and first mode shape ordinate at a given floor i. This mode shape is normalised to the roof level's value (i.e. $\phi_{roof} = 1$) since it corresponds to the location of the displacement Δ and can be found from a simple eigenvalue analysis of the structural model.

To evaluate the suitability of the proposed equivalent SDOF modelling approach shown in Fig. 4, some preliminary comparisons were conducted for the case study structures. These examined the model's overall ability to capture the global backbone response of the infilled and cracked RC frames. Comparisons of the hysteretic energy dissipated during a cyclic pushover analysis motion were also evaluated. Dolšek and Fajfar (2004) noted that the exact details of the hysteretic behaviour do not greatly affect the response of the model, a finding further bolstered by Kazantzi and Vamvatsikos (2018), but it was decided here to still try it, to be as representative as possible. These comparisons were conducted on all case study frames. Figure 5 displays the cyclic pushover results used to calibrate the equivalent SDOF model for one of the structures examined whereas Fig. 6 illustrates the difference in the hysteretic energy dissipated by the actual model and its 'equivalent' MDOF. This equivalent MDOF is obtained by transforming the force–displacement of the equivalent SDOF to the MDOF response ordinates via the same transformation factor, Γ, given in Eq. 4 so the actual model (in blue) is to be compared with the equivalent MDOF results only. For both cases, one can observe quite a good agreement in the response of the two models.

2.3 Assessment results

To evaluate the suitability of each of the aforementioned equivalent SDOF models (i.e. Approaches 1, 2 and the proposed approach) for dynamic analysis with respect to the response of the actual MDOF model of a structure, a series of IDAs were performed. The intensity measure selected for the purpose of this study was the spectral acceleration at the first mode period of vibration, $Sa(T1)$. A 5% Rayleigh damping model was adopted at the first and third modes of vibration for the actual model described in Sect. 2.1, as this

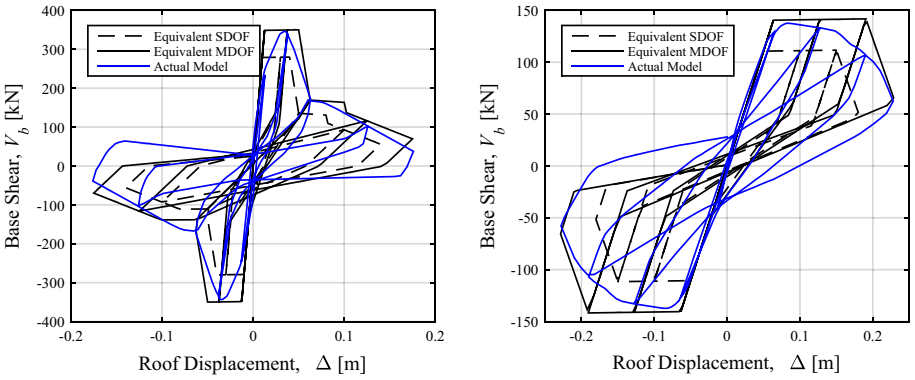

Fig. 5 Cyclic pushover curves showing the calibrated SDOF system to (left) actual model of infilled RC frame and (right) corresponding RC frame with infill at critical storey removed

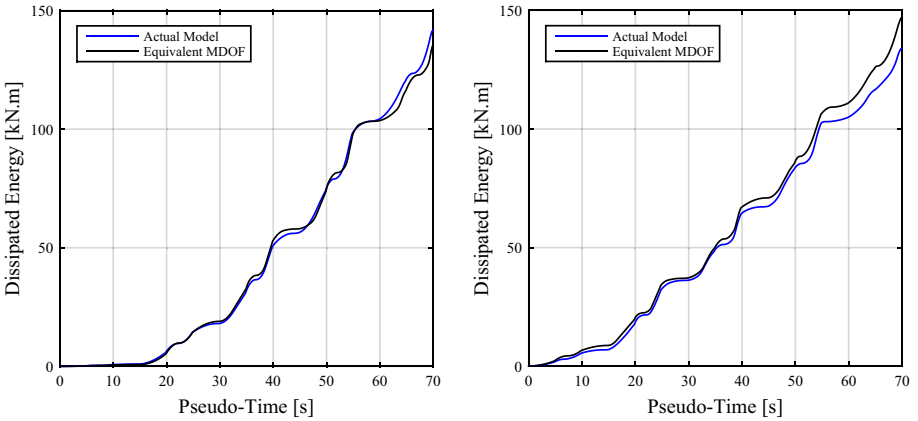

Fig. 6 Comparison of the dissipated hysteretic energy versus the pseudo-time of the SPO analysis for (left) the infilled RC frame and (right) its corresponding RC frame with infill at critical storey removed

replicates what was utilised by O'Reilly and Sullivan (2017) when comparing numerical simulations to experimental results. The set of ground motion records used to track the evolution of damage and response in the structure was the far-field ground motion set given in FEMA P695 (2009). IDA was conducted for each MDOF structure up until the complete collapse of the structures, which was taken to be when a 10% storey drift was observed in the dynamic analysis for a given record, as discussed by O'Reilly et al. (2018b). By taking the individual ground motion traces at each intensity, the median IDA trace (i.e. the 50% fractile) was computed and the comparison is represented in Fig. 7 for two of the structures examined. The results are normalised to show the strength ratio, R, and the ductility of the frames, μ, which are taken as the forces and displacements of the equivalent SDOF normalised to point 1 on Fig. 4.

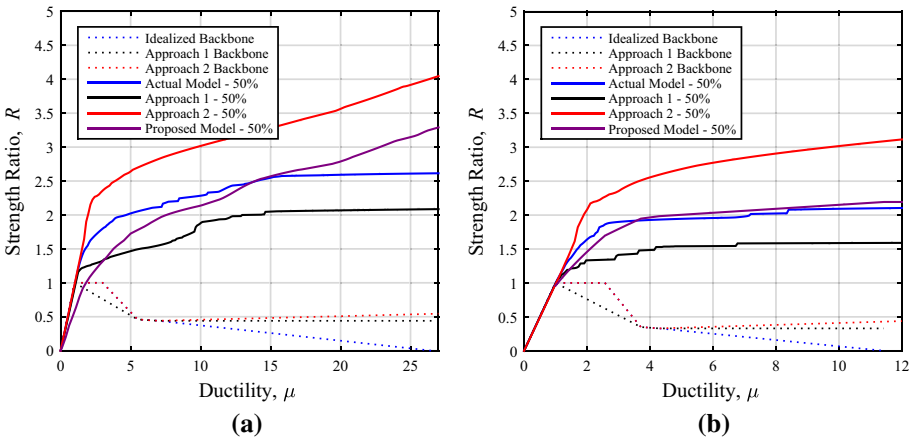

Fig. 7 Comparison of the median IDA curves normalised as R–μ using Approaches 1 and 2, the actual MDOF models and the proposed approach for **a** 2-storey weak-infilled frame, **b** 4-storey strong-infilled frame. The individual SPO oscillator backbones are also shown

Figure 7 illustrates the differences between Approaches 1 and 2 when compared to the response of the actual model for two of the case study structures examined. Approach 1 tends to overestimate the behaviour of the structure for a given intensity because of the model's oversimplification of the initial portion of the backbone curve shown in Fig. 2a. The use of a single peak point followed by a sharp drop in strength to model the effects of masonry infill tends to result in an increased flexibility and subsequently larger displacement demand compared to the actual model. Adopting a bilinear backbone RC frame response for Approach 2 in Fig. 2b is reflected with a continuation in resistance with increasing intensity. Since no failure point of the RC frame is defined, the SDOF oscillators can keep withstanding increased values of intensity without their IDA curves ever actually 'flat-lining'. Flat-lining means that for a small increase in intensity, a large increase in demand is observed essentially making the IDA traces flatten out and are typically taken as an indication of structural collapse. Figure 7 shows that neither of the two approaches reviewed from existing literature adequately captures the response of the infilled RC frames right up to collapse. On the other hand, for the SDOF model proposed here in Fig. 4, the median values are much more aligned with the median response of the actual model, especially the intensity at the collapse of the structures, indicating that the minor adjustments made to the simplified SDOF backbones were at the same time necessary and adequate. As such, even if demonstrated with only two of the case-study frames, given the significant differences observed in the collapse intensity estimation, it is believed that the numerical modelling approach proposed here for infilled RC frames should be the one adopted in studies of this sort.

3 Simplified assessment of infilled RC frames

3.1 Existing methods

The previous section discussed different approaches to characterise the seismic response of infilled RC frames via SDOF oscillators. These essentially stem from the equivalent SDOF conversion of the MDOF's SPO curve followed by the consideration of the hysteretic characteristics to permit a subsequent dynamic analysis. However, once this SPO curve has been characterised, it may be also convenient to use a series of simplified expressions to relate the SPO backbone to its dynamic response via ground motion excitation. These are commonly referred to as R–μ–T relationships since they provide the relationship between the strength ratio, R, the ductility, μ, and the period, T, which is usually defined as the first mode period, T_1. The strength ratio, R, is defined as:

$$R = \frac{F_{el}}{F_y} = \frac{Sa\left(T_1\right)}{Sa_y} \tag{5}$$

where F_{el} is the elastic spectral demand on a SDOF oscillator of period T_1 subjected to ground motion excitation, and F_y is the yield force of that oscillator. In other words, R essentially represents the ratio between the first-mode spectral acceleration value of a given ground motion or design spectrum, $Sa(T_1)$, and the yield spectral acceleration of the equivalent SDOF, Sa_y. There have been numerous studies on such relationships for different structural systems over the years (Veletsos and Newmark 1960; Newmark and Hall 1982; Vidic et al. 1994; Miranda 2000). Of particular pertinence to this study is the

aforementioned work by Dolšek and Fajfar (2004), who utilised the modelling approach described in Fig. 2b to quantify these relationships for infilled RC frames. These relationships worked well in comparison to actual results and were widely adopted in the literature for the simplified assessment of infilled RC frames. However, these relationships inherently contain each of the various limitations described in the equivalent SDOF modelling approach described in Sect. 2.2 and evaluated in Sect. 2.3. More specifically, they consider infinite ductility of the RC frames and are not expected to adequately capture its strength degradation and eventual collapse. Furthermore, these relationships provided the mean response and did not directly attempt to quantify variability. These latter two aspects were indirectly addressed in the development of the SPO2IDA tool by Vamvatsikos and Cornell (2005), as illustrated in Fig. 8, whereby the relationship between the SPO curve and its corresponding IDA fractiles (i.e. 16%, 50% or median and 84%) was quantified in an empirical manner.

SPO2IDA presents an attractive method to estimate the seismic demand and capacity of first-mode-dominated MDOF systems in regions ranging from near-elastic to global collapse. It has been primarily developed to analyse bilinear systems with some form of degradation, as shown in Fig. 8, which corresponds well to the behaviour of ductile moment frames, for example. However, in the case of existing RC frames, these tend to have masonry infills that significantly affect the structural behaviour by adding strength and stiffness, as illustrated in Fig. 3. This modified behaviour of the SPO curve is problematic when combining it with tools such as SPO2IDA as they were developed with R–μ–T relationships more suited to ductile systems typical of new construction. To overcome this, one may simply incorporate the simplified fits proposed by Dolšek and Fajfar (2004) but, as mentioned above, these have a number of aspects to be further developed before extension to IDA characterising the performance up to collapse can be captured.

3.2 Evaluation of performance

To evaluate the performance of the outlined simplified methods, both were implemented here for the infilled RC frames presented in Sect. 2.1 and compared with the results of the IDA conducted in Sect. 2.2 for the MDOF structures. In other words, the SPO curves were characterised as shown in Fig. 1, then the idealised backbones for the Dolšek and Fajfar (2004) model (Approach 2) were fitted and the R–μ–T relationships

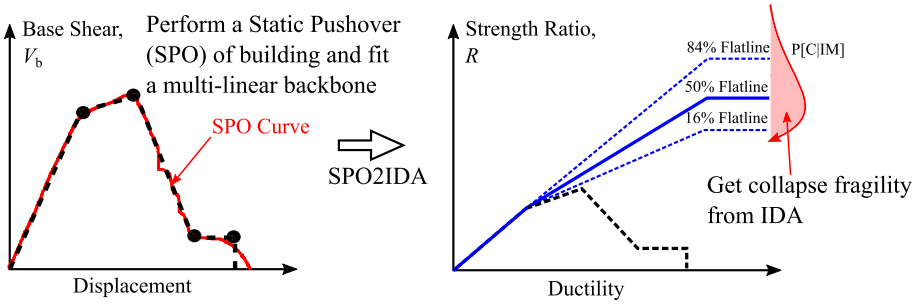

Fig. 8 Estimation of the IDA curves generated using the SPO2IDA tool developed by Vamvatsikos and Cornell (2005), whereby the relationship between the SPO backbone and the IDA fractiles is established with a library of empirical fits akin to the classic R–μ–T relationships

extrapolated to quantify the spectral acceleration required to reach a given level of ductility. The SPO2IDA tool by Vamvatsikos and Cornell (2005) was also implemented. By comparing these simplified results with those of the IDA of the MDOF, their effectiveness at quantifying the structural response up to collapse was evaluated. It is recalled that this comparison differs to that of Sect. 2.2 in that no dynamic analyses were conducted on the SDOF models and only simplifying R–μ–T relationships were utilised.

For the approach outlined by Dolšek and Fajfar (2004), a series of empirical relationships were used for quantifying a dynamic R–μ–T relationship for the mean response. For the case of SPO2IDA, two alternative approaches are permitted to carry out the equivalent SDOF conversion. These relate to using the transformation factor, Γ, described in Eq. 4 (for a more accurate definition) or by simply using the ratio between the yield force and the total weight of the system, C_0. The backbone shape illustrated in Fig. 8 was utilised for SPO2IDA, whereby the SPO is characterised by a bilinear system with some strength and stiffness reduction and residual strength plateau followed by eventual loss of capacity. It is important to note that the current SPO2IDA tool available in the literature models the final branch as a constant residual strength and not as a gradual strength degradation, which would be required for infilled RC frames like those shown in Fig. 1, where an additional strength plateau and gradual reduction occur (i.e. the first peak strength plateau of the infills, followed by their strength loss down to the next strength plateau of the infilled RC frame with the infill removed, and then the gradual strength reduction of the entire system to collapse). This constant strength branch is not a problem when analysing structures that can be characterised as bilinear with a single strength reduction and some minimal residual strength like the one shown in Fig. 8, but for infilled RC frames where two significant reductions in strength with increasing demand tend to occur, this can have large and undesirable consequences, as the final gradual degrading branch ends up being modelled as a constant strength branch in the tool. This limitation could be solved by adding another branch to the SPO2IDA backbone since the available backbone options end up being used in an unintended way when analysing infilled RC frames, which is elaborated further in Sect. 4. The results of this comparison are shown in Fig. 9 again for the two frames examined in Sect. 2.3.

When compared to the median response of the actual model, Fig. 9 shows that both SPO2IDA and Approach 2 tend to a reasonable match with the MDOF model curve for low ductility but once the response exceeds the first descending strength branch, they both begin to largely overestimate the strength ratio. In the case of Approach 2 by Dolšek and Fajfar (2004), this arises due to the assumption of infinite RC frame ductility, meaning that the SDOF oscillator possesses no physical means of losing its lateral capacity and can continue withstanding increased ground shaking. In the case of SPO2IDA, this overestimation is due to the limitation of the backbone parameters described above whereby a constant residual strength branch is considered instead of a gradually degrading one. Figure 9 shows that SPO2IDA clearly expresses an overestimation of the capacity since it has not been developed or adapted for these specific typologies, hence missing some of the key performance aspects towards collapse and post-peak branches. This is noted to be consistent with the initial findings of O'Reilly and Sullivan (2017) who reported that, when applied to infilled RC frames, SPO2IDA tended to largely overestimate the median collapse intensity when compared to IDA results, potentially leading to an unconservative prediction of the performance.

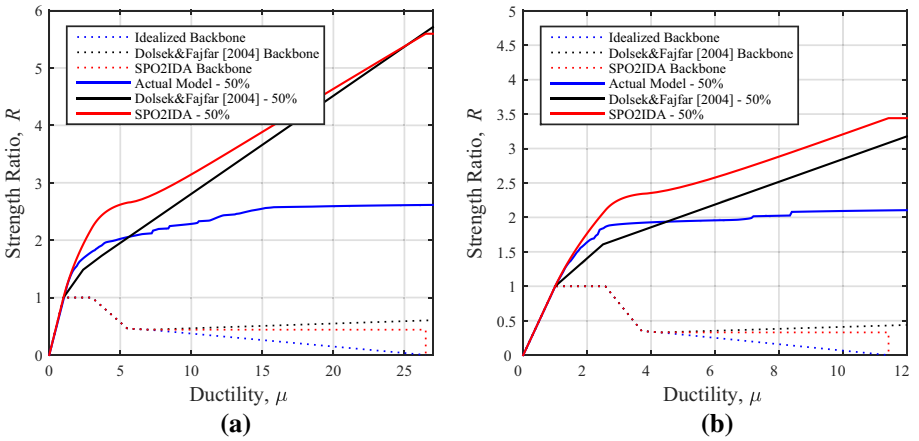

Fig. 9 Comparison of the R–μ median response using Approach 2, SPO2IDA and the actual MDOF models for **a** 2-storey weak-infilled frame, **b** 4-storey strong-infilled frame. The individual SPO curves and their assumptions with respect to the post-peak behaviour modelling are also shown for each case

4 Extension of simplified analysis via SPO2IDA to infilled RC frames

As seen in the previous sections, SPO2IDA offers a simple and effective solution to characterise the structural response to ground motion excitation with increasing intensity. However, Sects. 2 and 3 have demonstrated that there are still some aspects to be further developed before SPO2IDA can be confidently applied to infilled RC frame typologies to quantify their behaviour up to collapse. In this section, a large sample of representative SDOF systems were analysed using IDA in order to characterise their performance with increasing intensity and allow the fitting of a new empirical library of R–μ–T relationships. These are to be used in the context of a tool, such as SPO2IDA, whose output will resemble that of Fig. 10, where A–B represents the post-yielding or hardening branch, B–C the softening branch or where the rupture of infills occur, C–D the residual plateau due to the underlying RC frame's resistance and D–E the strength degradation branch presented

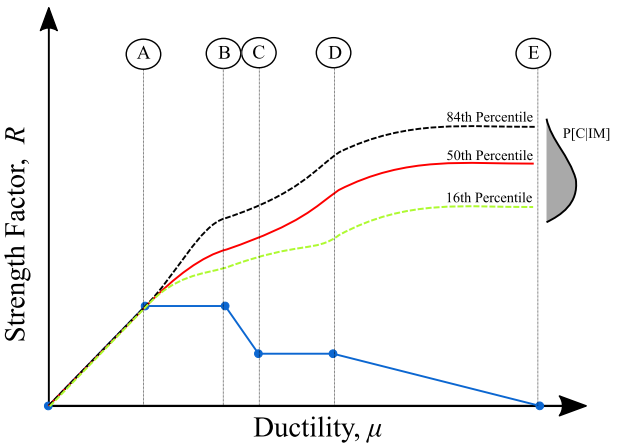

Fig. 10 Idealised strength ratio, R, versus ductility, μ, of a given infilled RC frame's equivalent SDOF

subsequently in Sect. 4, which differ from the arrangement of the assumed set of branches in original SPO2IDA tool. The end-result of this analysis is a new library of fits and hence an extended SPO2IDA version for infilled RC frames. Two-step regression was employed to establish and quantify the relationship between the dynamic strength ratio, R, and the ductility, μ, for a given SPO backbone specific to infilled RC frames.

4.1 Generation of parametric infilled RC frame structures

The first task was to establish a suitable database of case study structures and carry out a parametric quantification of infilled RC frame response with which to then conduct a two-step regression. As the purpose of SPO2IDA is to relate the response of an idealised SDOF oscillator to its SPO backbone (given the equivalent SDOF conversion in Sect. 2.2), the parametric study described herein only considered the response of SDOF oscillators.

To obtain a sufficient number of SDOF oscillators, a large database of SDOFs was randomly sampled to have a sufficient amount of combinations of potential SPO backbone shapes. As such, realisations of the structural models for a given number of random variables (RV), defined as the various points illustrated in Fig. 4, in addition to the equivalent SDOF's initial period, T^*, were generated. To do this, the correlation-controlled Latin hypercube sampling (CLHS), utilised in O'Reilly and Sullivan (2018), was employed to reduce spurious and unintentional correlations between the different RVs. The distributions of the various considered RVs were derived from the empirical data of the case study structures described in Sect. 2.1, as these were considered to represent a range of backbones typically found for such infilled RC frames. It is noted that by doing so, a number of inherent assumptions about the infilled RC frames' characteristics were made regarding aspect and slenderness ratio, in addition to and relevant strength ratios between the masonry infill and the RC frame. As such, the application of the tool developed herein may be considered limited to structures with similar characteristics as those examined in Sect. 2.1 and may require further refinement when significantly different. RVs associated with both the infilled RC frame and the frame with an induced soft-storey mechanism were established, which correspond to the various points illustrated in Fig. 4. Table 2 lists the distributions of the RVs, characteristic of infilled RC frames (i.e. points 0–1–2–3–4) and the structures with a mechanism formed at the weakest storey (i.e. points 0–5–6–7). To

Table 2 List of the RVs and their associated lognormal distribution parameters

RV	Symbol	Point on backbone	Median	Dispersion
1	T^* (s)	–	0.39	0.56
2	F^*_{yi} (kN)	1	419	0.38
3	F^*_{si} (kN)	3	172	0.24
4	F^*_{yc} (kN)	5	164	0.25
5	Δ^*_{yi} (m)	1	0.013	0.56
6	Δ^*_{hi} (m)	2	0.043	0.47
7	Δ^*_{si} (m)	3	0.053	0.31
8	Δ^*_{mi} (m)	4	0.170	0.25
9	Δ^*_{yc} (m)	5	0.021	0.37
10	Δ^*_{hc} (m)	6	0.069	0.26
11	Δ^*_{mc} (m)	7	0.170	0.24

ensure lognormality of each of the RVs, the Kolmogorov–Smirnov goodness-of-fit test was utilised and demonstrated the suitability of such a distribution for all RVs.

Each of the 11 RVs were sampled a number of times to generate 500 model realisations. While each of the RVs were sampled according to the aforementioned distributions and correlations, care was taken to ensure that no instances of unrealistic model realisations arise. This resulted in a set of 500 SPO backbones systems whose individual RV distributions, and corresponding correlations between each RV, matched that of the original set of case study structures. Furthermore, as shown in Fig. 11, the target correlation was achieved via CLHS as both the target correlation matrix and the actual correlation matrix were noted to be very similar. This was demonstrated by computing the norm to quantify the difference between correlation matrices, as outlined by Vorechovsky and Novak (Vorechovsky and Novak 2003), which when computed for the two matrices plotted in Fig. 11a, c, was observed to have a magnitude of 10^{-3} that was deemed acceptable.

4.2 Assessment of SDOF oscillators via IDA

Upon sampling the equivalent SDOFs, IDA was conducted in the same manner as Sect. 2.2 to perform a comprehensive assessment of the behaviour of such structures under seismic loads. These equivalent SDOF oscillators are shown in their entirety in Fig. 12, where the variability between the different oscillator parameters can be seen. As noted, the backbones presented in Fig. 12a are intended to represent the response of the infilled RC frame (i.e. the backbone composed of points 0–1–2–3–4 shown in Fig. 4) and the backbones presented in Fig. 12b represent the corresponding response of the structure once critical storey has formed a mechanism (i.e. the backbone composed of points 0–5–6–7 shown in Fig. 4). Therefore, these SDOF models comprise a combination of this Fig. 12b model and the infill contribution to give the Fig. 12a response initially but reduces to the Fig. 12b response once the infill has collapsed. Computational time and effort were relatively reduced as SDOF oscillators were utilised for these analyses as opposed to MDOF models. With these IDA results, the individual traces of each ground motion were then tracked with increasing demand to arrive at the quantification of the 16%, 50% or median, and 84% intensity fractiles, as illustrated previously in Fig. 10. These fractiles were then used to define the empirical relationship for each branch found via two-step regression, which will be detailed in the following sections.

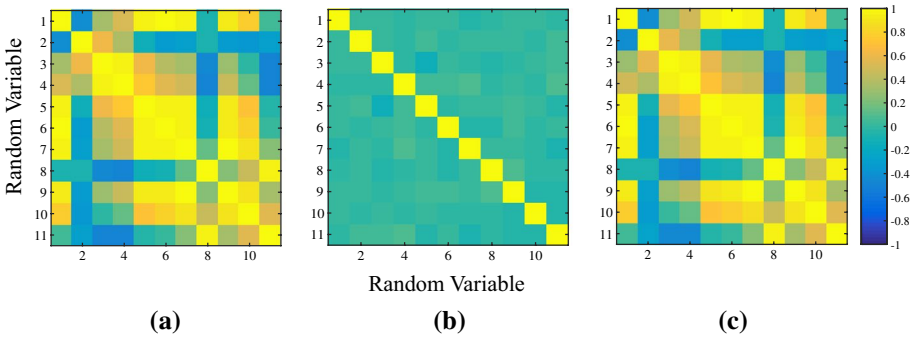

Fig. 11 Comparison of the **a** target correlation matrix, **b** correlation matrix without CLHS, **c** correlation matrix with CLHS utilised in this study

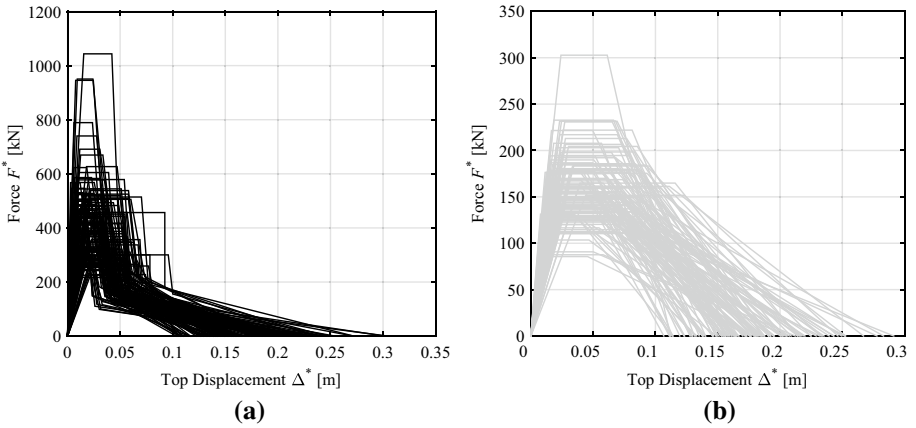

Fig. 12 Summary of the equivalent SDOF models sampled using CLHS where **a** illustrates the backbones of the infilled RC frames, **b** the backbones of the frames with a mechanism developed in the critical storey

4.3 Fitting of coefficients via two-step regression

Upon sampling the equivalent SDOF systems, individual IDAs were performed using the far-field ground motion dataset given by FEMA P695 for 5% damping. The SPO curves (i.e. F^* vs. Δ^*) and their respective IDA curves [i.e. $Sa(T^*)$ vs. Δ^*] were then normalised using F_y^* and Δ_y^* (determined by the user from the SPO curve) into a strength ratios R and ductility μ as follows:

$$R = \frac{F^*}{F_y^*} \tag{6}$$

$$R_{dyn} = \frac{Sa(T^*)}{Sa_y} \tag{7}$$

$$\mu = \frac{\Delta^*}{\Delta_y^*} \tag{8}$$

where R_{dyn} is simply used to distinguish the strength ratio established from IDA from that coming from the SPO curve; F_y^* and Sa_y are the yield base shear and yield spectral acceleration of the SDOF system, respectively, with:

$$Sa_y = \frac{4\pi^2 \Delta_y^*}{(T^*)^2} \tag{9}$$

First, the dynamic R–μ–T relationship was determined through correlating both the strength ratio R and the ductility μ using a parametric relationship that was found most suitable for the branch of response. Second, the initial period of the SDOF system was introduced as a proxy to quantify these relationships' coefficients. In other words, a R_{dyn}–μ relationship was determined first via a number of coefficients [e.g. $R_{dyn} = f(\mu, \alpha, \beta, \gamma)$] and then T^* was utilised to fit these coefficients [e.g. $\alpha = f(T^*)$]. The subsequent sections discuss the fitting models assumed

to be most adequate for each branch of the IDA response, referring to the models adopted in the existing tools when appropriate. Thus, R–μ–T relationships established as closed-form solutions along with their respective coefficients extracted following the process described above are provided. Upon concluding the fitting for each branch of the idealised SPO curve, the R_{dyn}–μ couple can be converted back to the MDOF system's response ordinates by the same equivalent transformation used previously in reverse, as follows:

$$Sa\left(T_1\right) = R_{dyn} Sa_y \Gamma \tag{10}$$

$$\Delta = \Gamma \cdot \mu \cdot \Delta_y^* \tag{11}$$

which is essentially an IDA curve. Using this process, knowing the idealised SPO curve and transformation factor Γ for an infilled RC frame, the proposed extended SPO2IDA algorithm can be outlined as follows:

1. For a ductility, μ, in a given branch of the SPO curve as shown in Fig. 10, the roof displacement of the MDOF, Δ, is found using Eq. 11;
2. The yield spectral acceleration, Sa_{y}, is found from Eq. 9;
3. Using the coefficients fitted for the x% fractile of the IDA for a certain branch of the IDA, the R_{dyn} is found and then converted to a spectral acceleration $Sa(T_1)$ using Eq. 10;
4. This process is repeated for each of the branches shown in Fig. 10, for each of the fractiles required (e.g. $x = 16\%$, 50% and 84%) to get an IDA curve similar to that illustrated in Fig. 10.

The following subsections describe the process that was followed to establish these fitting coefficients for each of the branches and the fitting models adopted for the different fractile values. The fitting models were established using goodness-of-fit statistics for parametric models in terms of: the sum of squares due to errors (SSE), R^2, adjusted R^2, and the root mean squared error (RMSE). These goodness-of-fit metrics quantify the deviation of the fit from the response and the error component in general and hence were deemed suitable to evaluate the fits.

4.3.1 Hardening branch

As noted by Vamvatsikos (2002) during the initial development of the SPO2IDA tool, fitting the hardening branch of the IDA curve is relatively straightforward and has been attempted by many others in the past (Veletsos and Newmark 1960; Newmark and Hall 1982; Vidic et al. 1994; Miranda 2000). Observing the data obtained from the IDA, a power law fit was adopted involving two parameters α_1 and β_1, as described in Eq. 12. This expression characterises the R–μ relationship obtained from the IDA and its coefficients α_1 and β_1 are derived using a 7-term Gaussian fit to the observed data and are thus expressed as a function of the fundamental period of the equivalent SDOF, T*, and are described by Eqs. 13 and 14

$$R_{dyn} = \alpha_1 \mu^{\beta_1} \tag{12}$$

$$\alpha_1 = \sum_{i=1}^{7} a_{\alpha 1,i} \exp\left(\frac{T^* \cdot b_{\alpha 1,i}}{c_{\alpha 1,i}}\right) \tag{13}$$

Table 3 Goodness of fit parameters for α_1 and β_1

Parameter	SSE	R^2	Adjusted R^2	RMSE
$\alpha_{1-16\%}$	1.358	0.785	0.777	0.0526
$\alpha_{1-50\%}$	0.926	0.751	0.741	0.0434
$\alpha_{1-84\%}$	1.218	0.726	0.715	0.0498
$\beta_{1-16\%}$	2.307	0.837	0.830	0.0686
$\beta_{1-50\%}$	1.254	0.895	0.891	0.0505
$\beta_{1-84\%}$	1.487	0.839	0.833	0.0550

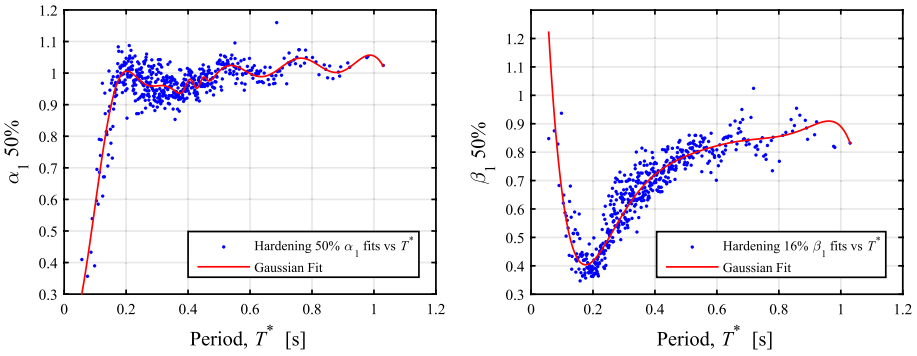

Fig. 13 Fitting of the terms (left) α_1 and (right) β_1 terms for the hardening branch of the 50% IDA fractile

$$\beta_1 = \sum_{i=1}^{7} a_{\beta 1,i} \exp\left(\frac{T^* \cdot b_{\beta 1,i}}{c_{\beta 1,i}}\right). \tag{14}$$

This fitting was conducted for each of the pertinent fractiles of the IDA (i.e. $x = 16\%$, 50% and 84% fractiles) and the coefficients are provided in Tables 8, 9, 10, 11, 12 and 13 of the "Appendix" section. The "goodness of fit" results summarised in Table 3 denote a satisfactory fit for the parameters and functions used to represent the hardening branch. The results of SSE, R^2 and the adjusted R^2 values express a good prediction model with relatively low error, respectively. To illustrate the suitability of these fitted functions for the hardening branch, a comparison between the IDA results data and the fitted function is illustrated in Fig. 13, where a satisfactory match can be seen.

4.3.2 Softening branch

The negative stiffness is found in the SPO infilled RC frames as it signals the loss in infill capacity and often the onset of a soft-storey mechanism. The most prominent feature of the negative branch is the characteristic flattening of the IDA curve, which results in a flatline unless it is impeded by the residual plateau. In comparison with the hardening branch, the fitting of the softening or negative slope branch of the median IDA response is somewhat trickier, especially upon the selection of the optimum mathematical model to consider. Hence, through observations, a 2nd order polynomial was deemed adequate for the representation of the behaviour, which is presented in Eq. 15

$$R_{dyn} = \alpha_2 \mu^2 + \beta_2 \mu + \gamma_2 \tag{15}$$

where α_2, β_2 and γ_2 are given in Eqs. 16–18

$$\alpha_2 = a_{\alpha 2} T^* + b_{\alpha 2} \tag{16}$$

$$\beta_2 = a_{\beta 2} T^* + b_{\beta 2} \tag{17}$$

$$\gamma_2 = a_{\gamma 2} T^* + b_{\gamma 2}. \tag{18}$$

As in the case of the hardening branch, the coefficients are provided for the 16%, 50% and 84% fractiles of the IDA in Table 14 of the "Appendix" section. The statistics attributed to the "goodness of fit" given in Table 4 denote a reasonable fit for the softening despite the fact that this branch is relatively difficult to quantify. The SSE for α_2 and β_2 are relatively low, hence a suitable prediction model is expected, but a relatively poor forecasting for γ_2 may be expected. R^2 and the adjusted R^2 values for all parameters ($\approx$99%) express a very low error and the RMSE statistics indicate a low fit standard error for all models. The fits are displayed in Fig. 14.

4.3.3 Residual plateau branch

The effect of the SPO residual plateau is to revive the IDA trace and allow it to move on to higher intensities, in an almost linear-system-like manner (Vamvatsikos 2002). The expression used to represent the residual strength branch is characterised by a linear relationship as presented in Eq. 19

$$R_{dyn} = \alpha_3 \mu + \beta_3 \tag{19}$$

where α_3 and β_3 are given by the 3-term Gaussian model as:

$$\alpha_3 = a_{\alpha 3} \cdot T^{*3} + b_{\alpha 3} \cdot T^{*2} + c_{\alpha 3} \cdot T^* + d_{\alpha 3} \tag{20}$$

$$\beta_3 = a_{\beta 3} \cdot T^{*3} + b_{\beta 3} \cdot T^{*2} + c_{\beta 3} \cdot T^* + d_{\beta 3} \tag{21}$$

and the coefficients are provided for the 16%, 50% and 84% fractiles of the IDA in Tables 15 and 16 of the "Appendix" section. The Gaussian function was employed for the

Table 4 Goodness of fit parameters for α_2, β_2 and γ_2

Parameter	SSE	R^2	Adjusted R^2	RMSE
$\alpha_{2-16\%}$	0.3755	0.9921	0.9921	0.0271
$\alpha_{2-50\%}$	0.1221	0.9924	0.9924	0.0155
$\alpha_{2-84\%}$	0.0563	0.9928	0.9928	0.0105
$\beta_{2-16\%}$	14.81	0.9920	0.9920	0.1704
$\beta_{2-50\%}$	6.639	0.9898	0.9898	0.1141
$\beta_{2-84\%}$	2.403	0.9926	0.9926	0.0686
$\gamma_{2-16\%}$	48	0.9902	0.9902	0.3068
$\gamma_{2-50\%}$	29.71	0.9837	0.9836	0.2414
$\gamma_{2-84\%}$	13.46	0.9858	0.9857	0.1625

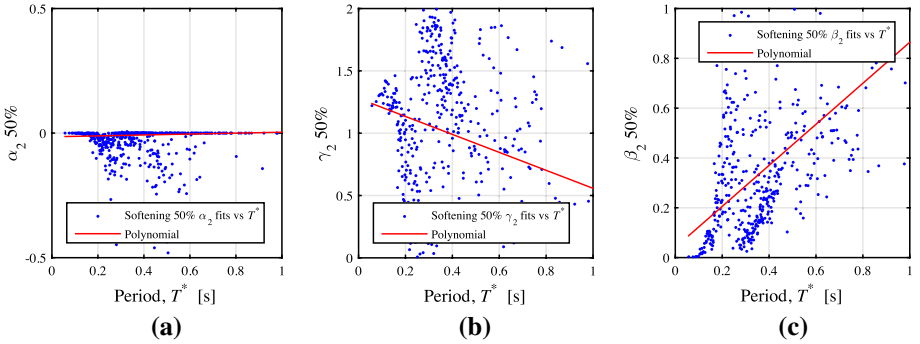

Fig. 14 Fitting of the terms for **a** α_2, **b** β_2, **c** γ_2 terms for the softening branch of the 50% IDA fractile

fitting of the parameters since it displayed more suitable results into fitting a fairly more complicated scatter. The "goodness of fit" results summarised in Table 5 denote a satisfactory fit for the parameters and functions used to represent the residual strength branch. The results of SSE, R^2 and the adjusted R^2 values express respectively a good prediction model with a low error component. The estimation of the random component's standard deviation via the RMSE statistic is also associated with a low fit standard error.

4.3.4 Strength degradation branch

The residual plateau of infilled RC frames is then followed by a strength degradation branch. The consideration of this branch in the quantification of R–μ–T for infilled RC frames represents one of the key developments of this work, where previous work such as that by Dolšek and Fajfar (2004) did not consider strength degradation, meaning that the structural behaviour up until structural collapse could not be captured, as illustrated previously in Fig. 9. The strength degradation branch is a simple linear R–μ relationship and is given by:

$$R_{dyn} = \alpha_4 \mu + \beta_4 \tag{22}$$

where α_4 and β_4 are given by:

$$\alpha_4 = a_{\alpha 4} T^{*3} + b_{\alpha 4} T^{*2} + c_{\alpha 4} T^* + d_{\alpha 4} \tag{23}$$

$$\beta_4 = a_{\beta 4} T^{*3} + b_{\beta 4} T^{*2} + c_{\beta 4} T^* + d_{\beta 4} \tag{24}$$

Again, the coefficients are provided for the 16%, 50% and 84% fractiles of the IDA in Table 17 of the "Appendix" section. The statistics computed for the "goodness of fit" of the polynomials attributed for the fitting of the models and the factors employed in the fitting are summarised in Table 6 and illustrated in Fig. 16.

4.4 Summary

In general, the fits adopted for all four branches of the response represent a good basis for an approximate analysis of the infilled RC frame typology via an extended SPO2IDA, especially around the expected fundamental period T_1 of the said typology (typically

$0.1 < T_1 < 0.6$ s), considering the large stiffness value imposed by the addition of masonry infills. This simplified methodology presents a good estimate of the dynamic structural capacity of these structures without any given information of the infills strength. The analysis thus utilises relatively simple parameters to perform the approximate analysis (knowing base shear-displacement and fundamental characteristics of the structure, T_1, floor masses, and the first-mode shape profile, ϕ_1) via the extended SPO2IDA tools. This extended version of the tool described in the previous subsections has been implement both in a MS Excel Spreadsheet and a MATLAB script, which are available at https://github.com/gerardjoreilly/InfilledRC-SPO2IDA.

5 Verification of extended SPO2IDA for infilled RC frames

The proposed extension to SPO2IDA for infilled RC frames presented in Sect. 4 was tested for the case-study frames chosen initially for the study. The verification of the newly proposed coefficients was checked in terms of comparing IDA curves of the actual models presented previously and those acquired through the extended SPO2IDA tool. Furthermore, a risk-based comparison of the demand-exceedance curves using the existing SPO2IDA tool for general structures discussed in Sect. 3 was examined with respect to the extended tool and the actual IDA results to illustrate the potential impacts of mischaracterising the IDA curves on the risk-based quantities. Finally, an independent validation using the results from an existing RC frame school building with masonry infills located in Central Italy was also conducted.

5.1 Comparison of IDA curves for case study frames with extended SPO2IDA

By taking the IDA fractiles for each of the case study structures described in Sect. 2 and comparing with the extended SPO2IDA's prediction, the adequacy of the tools was evaluated generally. Figure 17 shows this for the case study structures, where the plots are normalised to strength ratio and ductility. For both cases, the IDA curves obtained from the extended SPO2IDA match well with the trends and the general range of strength demand exhibited by the traditional IDA of the actual models. Changes in the peak deformation or ductility patterns are preserved when comparing both to along with onset of stiffness, hardening and the other branches of the idealised backbone curve in Fig. 17, up until the strength degradation and eventual collapse.

5.2 Evaluation of drift-exceedance curves computed using extended SPO2IDA

A key element in using SPO2IDA is the capability to provide accurate estimates and properly define necessary aspects required in the broader scheme of performance-based earthquake engineering. The comparison of the extended SPO2IDA for infilled RC frames proposed here was also examined for its estimation of the mean annual frequency of exceedance (MAFE), λ, for a given limit value of a specific engineering demand parameter (EDP). Therefore, an arbitrary seismic hazard $H(s)$ (i.e. mean annual rate of exceedance of a given ground shaking intensity, s) is adopted as defined by Vamvatsikos (2013) where the hazard model coefficients were taken from a site in Italy with moderate seismicity examined in O'Reilly et al. (2018c), for the purposes of illustration. The expression of the MAFE of a given EDP, subsequently chosen to be the roof drift, θ (i.e. roof

displacement normalised by the total height), was computed using the closed-form solution also described in Vamvatsikos (2013), which has also been recently extended for bilinear deman-intensity models typical of infilled RC frames by O'Reilly and Monteiro (2019). The aleatory uncertainty associated with record-to-record variability was taken from the IDA fractiles, whereas the epistemic uncertainty was not considered for the sake of simplicity in this comparative exercise.

Figure 18 demonstrates the MAFE, λ, versus roof drift, θ, for two of the case-study frames previously illustrated. The two results for MAFE computed using the existing SPO2IDA are due to the available options to compute the yield spectral acceleration, Sa_y. SPO2IDA employs two methods: the first calculates Sa_y as being the ratio between the yield force, V_{by}, and the total weight of the frame, W, to give a coefficient (termed the F/W method in the tool), and the second computes it using a coefficient C_0 obtained from eigenvalue analysis via Eq. 9. The first method is the simplest but may prove to be inaccurate due to its approximate nature, while the second provides a more accurate solution using eigenvalue analysis results.

Figure 18 illustrates MAFE using the different simplified approaches (i.e. existing or extended SPO2IDA) comparison with IDA. The advantage of comparing the different approaches in terms of MAFE is that it takes the median response and its variability into account to give a value of direct relevance in performance-based assessment. For both cases of the existing SPO2IDA, the difference in MAFE is notable, especially at drift levels far from collapse. This is as a combined result of three factors: (1) the different R–μ–T relationships implemented in the existing SPO2IDA were not derived for infilled RC frame typologies; (2) the difference in computing Sa_y, where the F/W method is seen to provide the worse matching of the two, which is to be expected due to its simplicity; and (3) the lack of an additional residual strength branch before eventual strength degradation to capture the response of the infilled RC frames better. It tends to overestimate the capacity of the infilled RC frames at collapse and hence predict a lower collapse risk, meaning that depending on the options chosen in the existing tool, very unconservative predictions of collapse may result. The C_0 method is a substantial improvement but is seen to still deviate from the IDA results. For the extended SPO2IDA proposed here, one can clearly observe that the trend established and the range of values of the MAFE are well preserved, both because of the new library of R–μ–T relationships, the use of the C_0 method and the inclusion of an additional fitting branch illustrated in Fig. 10.

Considering this and the comparison of the IDA traces in the previous section, it can therefore be noted that the extended SPO2IDA presented in this study is in fact able to replicate the results obtained using extensive non-linear dynamic analysis while cutting down on computational time and effort, without compromising the response and its associated risk-based metrics.

5.3 Validation of extended SPO2IDA using existing school building in Italy

The building chosen to validate the results obtained using the extended SPO2IDA was a 3-storey RC school building with masonry infills located in Central Italy. The school building considered for the validation herein was constructed in the 1960s before the introduction of seismic design provisions and has previously been examined in detailed by O'Reilly et al. (2018c, 2019). The structural layout and general numerical modelling features are illustrated in Fig. 19, where the numerical modelling assumptions were similar to those adopted in this study.

SPO analysis was performed to quantify the building's response in both directions and the results are illustrated in Fig. 20. The highlighted points present the fitted linearisation to the SPO curves previously described in Fig. 4, which are needed as input to the extended SPO2IDA developed here. Multiple stripe analysis was conducted to assess the dynamic response of the structure with increasing levels of intensity at different return periods using different sets of hazard-consistent ground motion sets selected for a site in Central Italy, which are described more detail in O'Reilly et al. (2018c). The parameters needed to perform the MDOF to SDOF conversion in the extended SPO2IDA were determined from eigenvalue analysis, and are detailed in Table 7, following the equivalent SDOF conversion steps outlined in Sect. 2.2 and Eq. 9.

Using the MSA results for this school building, the performance of the school was quantified at a number of intensity levels, with some collapse cases noted for higher return period. The median collapse intensity and the dispersion due to record-to-record variability were deduced using a maximum likelihood approach by counting the number of collapse cases with respect to increasing intensity, as outlined by Baker (2015), and these were determined to be 1.63 g and 0.37, respectively.

Furthermore, two additional limit states corresponding to the peak resistance and the end of the residual plateau (point 3 in Fig. 4) were defined in order to compare the extended SPO2IDA and the MSA results. Roof displacements corresponding to these limit states (LS1 and LS2 herein) were identified in both principal directions of the school building and their exceedance with respect to increasing intensity was established from the MSA results. Similar to the collapse cases above, fragility functions were fitted and are reported in Fig. 21 for both directions. Using the SPO curves shown in Fig. 20 and the modal parameters described in Table 7 for both directions, the 16%, median and 84% IDA fractiles were established until collapse via the extended SPO2IDA. Using these traces, the associated fragility function for each limit state previously described could be established. These were identified and are also plotted in Fig. 21. Comparing the fragility functions, a good match is observed between the two sets in both directions of the building. This is true both in terms of the median intensity required to exceed each of these performance limit states and also the level of dispersion.

5.4 Discussion

The previous sections have illustrated that the proposed extension to the SPO2IDA tool for infilled RC frames is indeed sufficiently accurate to be used generally. Some aspects worth noting that were not mentioned previously are discussed here.

The first aspect is the inclusion of the period of vibration of the numerical model with the critical storey mechanism formed (i.e. systems plotted in Fig. 12b). This was also considered as a predictor variable for the α, β and γ terms discussed in Sect. 4.3 since the fragility analysis by O'Reilly et al. (2018a) suggested that this period may in fact be better correlated to the response of infilled RC frames once the mechanism has been formed. This was initially considered in the coefficient formulations, but no significant advantage was observed in terms of reducing the fitting error and was therefore not considered further. This may be investigated more thoroughly in the future to establish whether or not more refined estimates can be gained through its incorporation in the regression.

Other issues to consider are the scope and limitations of the proposed extension. The fitting was conducted on equivalent SDOF models with periods ranging between 0.1 and 1.0 s, with few cases above 0.6 s characterised by high variability in the fits

(see Figs. 13, 14, 15, 16). Therefore, the proposed tool is not recommended for application to structures with fundamental periods outside of that range of 0.1–0.6 s. Similarly, the analysis was conducted for 5% damping, limiting the application of this tool to structures with a similar assumption. It is worth noting that the extended SPO2IDA does not take into account the coupling of both directions in the background as it was primarily developed using equivalent SDOF systems. Moreover, hazard-consistency was not considered in the development due to the simplified nature of the approach, hence the use of a single set of ground motions. Additional sets of ground motions with different characteristics may also be considered in future refinements of the tool.

The simplified tool is only applicable for structures that are first-mode-dominant due to the assumptions used during the MDOF to SDOF transformation describe in Sect. 2.2. This means that the influence of higher modes on the response of the structure are not incorporated. This aspect was also discussed by Baltzopoulos et al. (2017) who noted that one way to address this limitation would be to indirectly account for these higher mode effects through the 'injection' of additional variability in the quantified effects. This approach was not discussed here but remains a viable option to address this issue.

Lastly, in terms of variability, only the aleatory uncertainty due to record-to-record variability has been incorporated in the implementation of the extended SPO2IDA tool. Other sources of uncertainty modelling uncertainty should be incorporated when utilising the results.

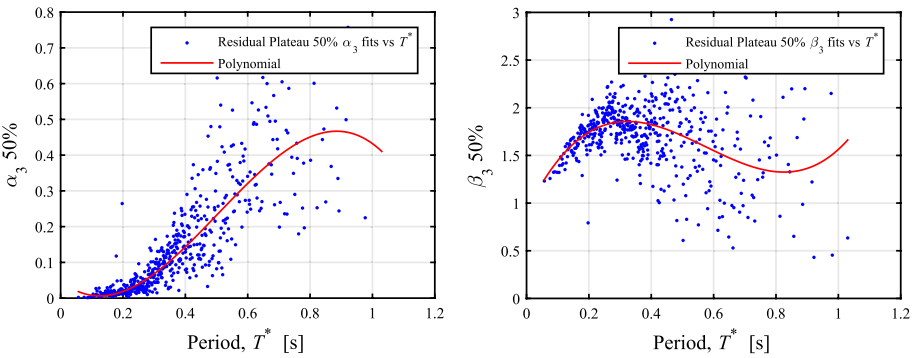

Fig. 15 Fitting of the terms α_3 (left) and β_3 (right) terms for the residual plateau branch of the 50% IDA fractile

Table 5 Goodness of fit parameters for α_3 and β_3

Parameter	SSE	R^2	Adjusted R^2	RMSE
$\alpha_{3\text{–}16\%}$	0.327	0.9920	0.9919	0.02537
$\alpha_{3\text{–}50\%}$	0.1062	0.9907	0.9906	0.01446
$\alpha_{3\text{–}84\%}$	0.03557	0.9856	0.9855	0.00837
$\beta_{3\text{–}16\%}$	5.334	0.9771	0.9771	0.10250
$\beta_{3\text{–}50\%}$	1.686	0.9734	0.9733	0.05761
$\beta_{3\text{–}84\%}$	0.625	0.9745	0.9744	0.03508

Table 6 Goodness of fit parameters for α_4 and β_4

Parameter	SSE	R^2	Adjusted R^2	RMSE
$\alpha_{4-16\%}$	0.03268	0.9942	0.9942	0.008021
$\alpha_{4-50\%}$	0.00723	0.9927	0.9927	0.003773
$\alpha_{4-84\%}$	0.002886	0.9898	0.9898	0.002384
$\beta_{4-16\%}$	6.344	0.976	0.9759	0.1118
$\beta_{4-50\%}$	1.348	0.9852	0.9851	0.05152
$\beta_{4-84\%}$	0.4172	0.9872	0.9871	0.02866

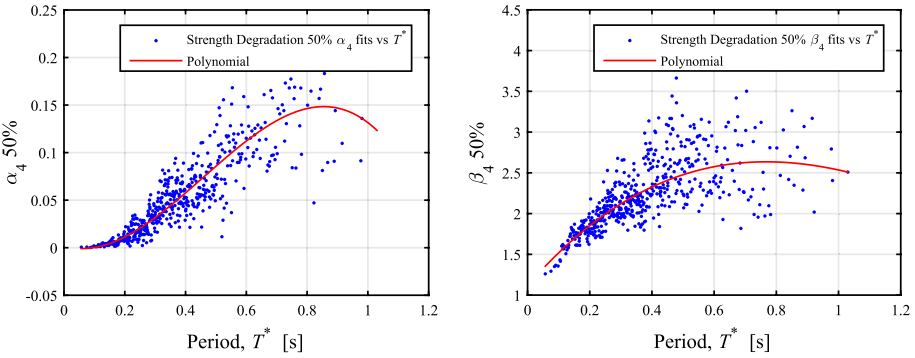

Fig. 16 Fitting of the terms α_4 (left) and β_4 (right) terms for the strength degradation branch of the 50% IDA fractile

6 Summary and conclusions

The seismic assessment of existing reinforced concrete (RC) structures with masonry infills remains a noteworthy topic in earthquake engineering. The quantification of their behaviour with respect to increasing intensity is a critical aspect when evaluating the risk associated with such structures in the broader scheme of performance-based earthquake engineering. Non-linear dynamic analyses procedures like incremental dynamic analysis (IDA) are demanding procedures in terms of the large computational effort and time required when performed on detailed numerical models built to capture the potential failures models pertinent in these structural typologies. This study has reviewed simplified approaches to assess structures, paying particular attention to methods applicable to RC structures with masonry infills. These approaches comprised both equivalent single degree of freedom (SDOF) oscillators and their definition and empirical relationships, often referred to R–μ–T relationships. As a result of this study, the following can be noted:

- Existing approaches to characterise the response of infilled RC frames via equivalent SDOFs are not entirely representative when compared to the response of detailed numerical models. This stemmed from the simplifications made when characterising the backbone behaviour in addition to the incorporation of a strength degradation and eventual collapse of the structure. A more refined equivalent

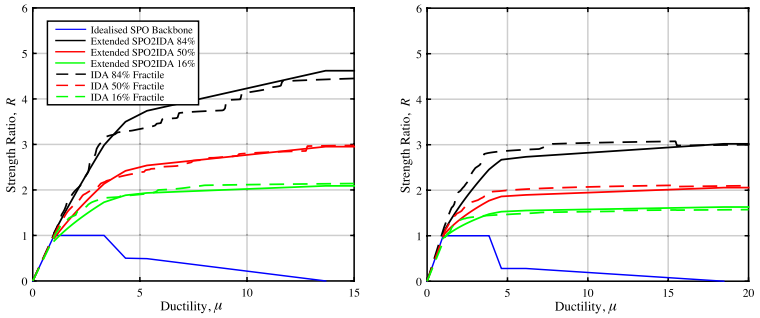

(a) 3-storey weak-infilled frame **(b)** 3-storey strong-infilled frame

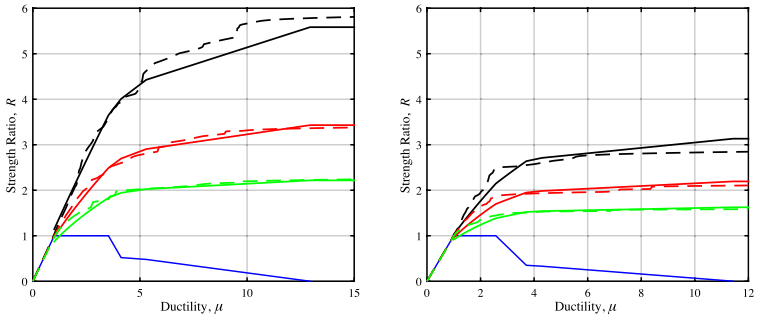

(c) 4-storey weak-infilled frame **(d)** 4-storey strong-infilled frame

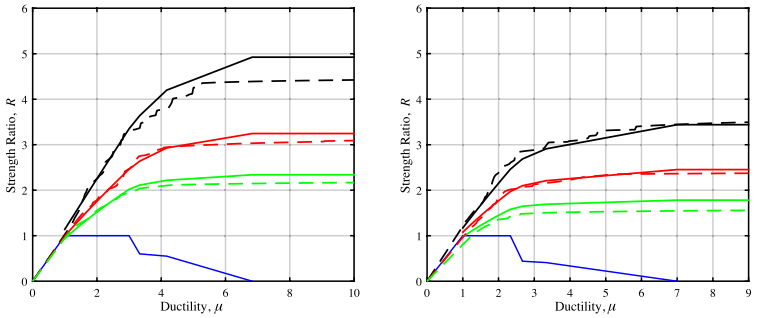

(e) 6-storey weak-infilled frame **(f)** 6-storey strong-infilled frame

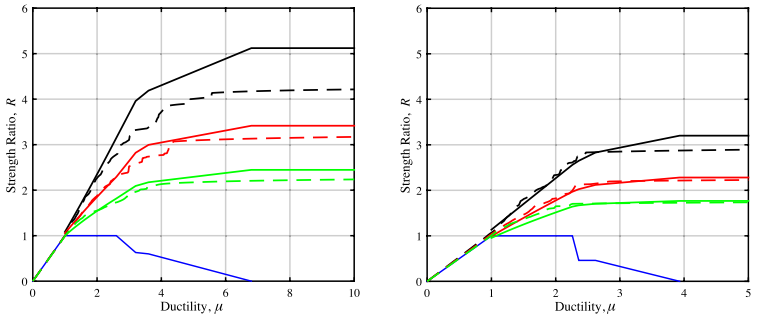

(g) 9-storey weak-infilled frame **(h)** 9-storey strong-infilled frame

Fig. 17 Comparison of the R–μ fractiles (16%, 50% and 84%) response using IDA on the actual MDOF models and the extended SPO2IDA

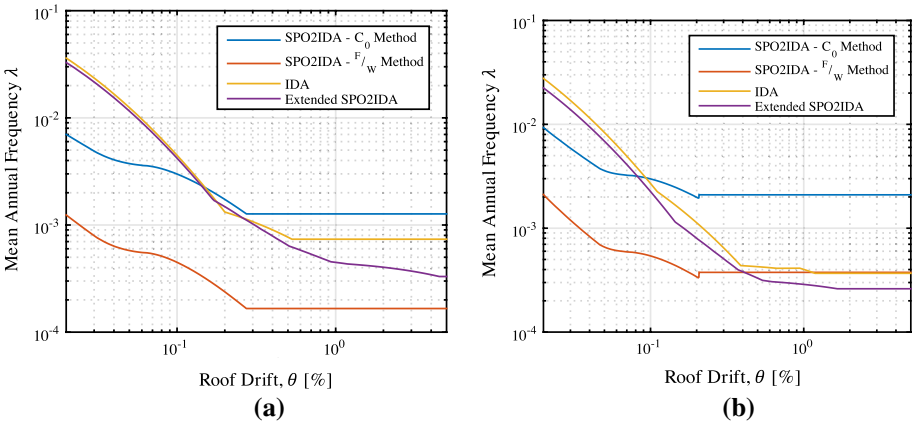

Fig. 18 Comparison of the MAFE, λ, for roof drift, θ computed using IDA on the MDOF model, the existing SPO2IDA for two approaches to compute Sa_y and using the extended SPO2IDA proposed in this study for **a** 2-storey weak-infilled frame, **b** 4-storey strong-infilled frame

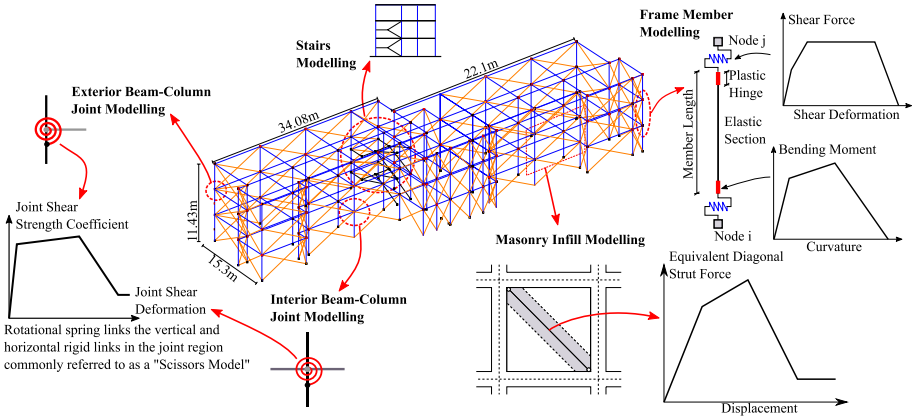

Fig. 19 General layout and numerical modelling assumptions of the case study school building located in Central Italy. Adapted from O'Reilly et al. (2019)

SDOF modelling approach was subsequently proposed and seen to characterise the global behaviour of such structures quite well up to collapse;

- The applicability of the tool relating the static pushover (SPO) curve of a structure to its IDA fractiles (SPO2IDA) was reviewed and seen not to be applicable to RC frames with masonry infills. This was seen to be due to the assumptions made regarding SPO backbone branches in the original tool that do not fit well with the specific characteristics of infilled RC frames;
- An extended SPO2IDA tool was subsequently developed, where the response of infilled RC frames characterised by a simplified backbone fit characteristic of their behaviour was utilised. A new library of R–μ–T relationships were fitted to the IDA results via a two-step regression;

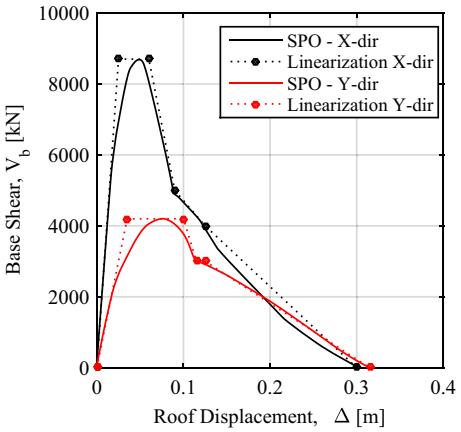

Fig. 20 SPO curves of the case-study building in both principal directions including the fitted linearised model proposed in this study

Table 7 MDOF to SDOF conversion parameters from eigenvalue analysis

X-direction				Y-direction			
T_1 (s)	m^* (kg)	Γ	Sa_y (g)	T_1 (s)	m^* (kg)	Γ	Sa_y (g)
0.365	1572.83	1.35	0.673	0.621	1554.49	1.35	0.193

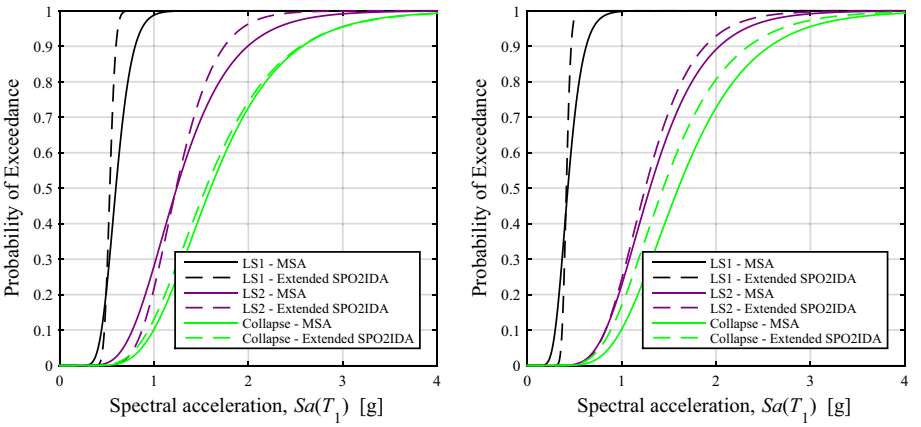

(a) X-direction **(b)** Y-direction

Fig. 21 Comparison of the fragility functions derived for three exemplary limit states including the collapse of the school building obtained via MSA and the extended SPO2IDA tool

- This extended SPO2IDA was then compared to the actual IDA results of case study structures, both in terms of IDA traces and risk-based quantities, where a good matching was observed in each case. Furthermore, comparison of the results with an independent study on an existing school building in Central Italy of the same typology further verified the applicability of this simplified tool for the collapse assessment and general characterisation of their structural response.

Table 8 Fitted coefficients for the α_1 term, each corresponding to the 50% values

i	$a_{\alpha 1,i}$	$b_{\alpha 1,i}$	$c_{\alpha 1,i}$
1	0.8628	0.7624	0.1643
2	0.9235	0.5041	0.1701
3	0.9195	0.1785	0.1147
4	0.9632	1.0220	0.1694
5	0.4745	0.3253	0.0940
6	0.0654	0.4064	0.0205
7	0.0446	0.4479	0.0158

Table 9 Fitted coefficients for the α_1 term, each corresponding to the 16% values

i	$a_{\alpha 1,i}$	$b_{\alpha 1,i}$	$c_{\alpha 1,i}$
1	0.1460	0.5335	0.0344
2	0.5926	0.4161	0.3194
3	0.0731	0.4495	0.0167
4	0.2965	0.2215	0.1087
5	0.0269	0.3699	0.0158
6	1.0630	1.0030	0.6460
7	0.3127	0.1462	0.0718

Table 10 Fitted coefficients for the α_1 term, each corresponding to the 84% values

i	$a_{\alpha 1,i}$	$b_{\alpha 1,i}$	$c_{\alpha 1,i}$
1	1.024	0.9018	0.6555
2	0.6034	0.1928	0.1072
3	0.2466	0.4758	0.1232
4	0.0614	0.6903	0.0566
5	0.2511	0.3254	0.0707
6	0.0001	0.9390	0.0013
7	0.0709	0.3948	0.0229

Acknowledgements The work presented in this paper has been developed within the framework of the project "Dipartimenti di Eccellenza", funded by the Italian Ministry of Education, University and Research at IUSS Pavia. The first author gratefully acknowledges the support of the ReLUIS Consortium for this research via Line 7 of the ReLUIS/DPC 2014-2018.

Appendix

The following are the tables of the coefficients fitted via two step regression in Sect. 4.3.

For the α_1 and β_1 terms defined in Eqs. 13 and 14, Tables 8, 9, 10, 11, 12 and 13 provide the fitted coefficients, respectively, which are presented for the 16%, 50% and 84% IDA fractiles.

Table 11 Fitted coefficients for the β_1 term, each corresponding to the 50% values

i	$a_{\beta 1,i}$	$b_{\beta 1,i}$	$c_{\beta 1,i}$
1	−0.1334	0.7771	0.04907
2	0.3312	0.7647	0.00098
3	0.7985	0.0428	0.09365
4	0.0000	0.5721	0.0000
5	0.1543	0.4788	0.1050
6	0.9252	0.8165	0.5100
7	0.2809	0.3003	0.1216

Table 12 Fitted coefficients for the β_1 term, each corresponding to the 16% values

i	$a_{\beta 1,i}$	$b_{\beta 1,i}$	$c_{\beta 1,i}$
1	0.2008	1.0930	0.5405
2	0.1790	0.7169	0.0884
3	0.1425	0.4876	0.0496
4	0.1533	0.5709	0.0726
5	3.623e+12	97.610	17.940
6	0.0945	0.4424	0.0626
7	0.1964	0.3345	0.0952

Table 13 Fitted coefficients for the β_1 term, each corresponding to the 84% values

i	$a_{\beta 1,i}$	$b_{\beta 1,i}$	$c_{\beta 1,i}$
1	0.7182	0.04151	0.09018
2	0.1320	0.6058	0.04845
3	0.1233	0.4904	0.04392
4	0.0981	0.5448	0.01778
5	0.1429	0.3652	0.09815
6	0.6547	0.8431	0.71260
7	0.0001	0.7115	0.00018

For the α_2, β_2 and γ_2 terms defined in Eqs. 16–18, Table 14 provides the fitted coefficients, which are presented for the 16%, 50% and 84% IDA fractiles.

Table 14 Fitted coefficients for the α_2, β_2 and γ_2 terms

	16%	50%	84%
$a_{\alpha 2}$	0.0395	0.0183	0.00951
$b_{\alpha 2}$	−0.0307	−0.0148	−0.00782
$a_{\beta 2}$	1.0490	0.8237	0.4175
$b_{\beta 2}$	0.2494	0.0408	0.03164
$a_{\gamma 2}$	−0.7326	−0.7208	−0.0375
$b_{\gamma 2}$	1.1160	1.2790	1.0790

Table 15 Fitted coefficients for the α_3 term, each corresponding to the 16%, 50% and 84% values

i (%)	$a_{\alpha3,i}$	$b_{\alpha3,i}$	$c_{\alpha3,i}$	$d_{\alpha3,i}$
16	− 5.075	7.112	− 1.572	0.1049
50	− 2.099	3.182	− 0.6989	0.0481
84	− 0.382	0.6334	− 0.051	0.0020

Table 16 Fitted coefficients for the β_3 term, each corresponding to the respective 16%, 50% and 84% values

i (%)	$a_{\beta3,i}$	$b_{\beta3,i}$	$c_{\beta3,i}$	$d_{\beta3,i}$
16	16.16	− 26.50	10.92	1.0550
50	8.417	− 14.51	6.750	0.9061
84	− 0.027	− 1.80	2.036	1.0670

Table 17 Fitted coefficients for the α_4, β_4 and γ_4 terms

	16%	50%	84%
$a_{\alpha4}$	− 1.564	− 0.5954	− 0.0670
$b_{\alpha4}$	2.193	0.8170	0.1420
$c_{\alpha4}$	− 0.352	− 0.0919	0.0124
$d_{\alpha4}$	0.0149	0.00182	− 0.00201
$a_{\beta4}$	1.756	0.7315	− 0.4080
$b_{\beta4}$	− 8.719	− 3.7030	− 1.3330
$c_{\beta4}$	8.285	4.3910	2.5210
$d_{\beta4}$	1.198	1.1160	1.0580

For the α_3 and β_3 terms defined in Eqs. 20 and 21, Tables 15 and 16 provide the fitted coefficients, respectively, which are presented for the 16%, 50% and 84% IDA fractiles.

For the α_4, β_4 and γ_4 terms defined in Eqs. 23 and 24, Table 17 provides the fitted coefficients, which are presented for the 16%, 50% and 84% IDA fractiles.

References

Baker JW (2015) Efficient analytical fragility function fitting using dynamic structural analysis. Earthq Spectra 31(1):579–599. https://doi.org/10.1193/021113EQS025M

Baltzopoulos G, Baraschino R, Iervolino I, Vamvatsikos D (2017) SPO2FRAG: software for seismic fragility assessment based on static pushover. Bull Earthq Eng. https://doi.org/10.1007/s10518-017-0145-3

CNR (2014) Istruzioni per la Valutazione Affidabilistica della Sicurezza Sismica di Edifici Esistenti. CNR—Commissione Di Studio per La Predisposizione e l'analisi Di Norme Tecniche Relative Alle Costruzioni

Cornell CA, Krawinkler H (2000) Progress and challenges in seismic performance assessment. PEER Center News 3(2):1–2

Crisafulli FJ, Carr AJ (2007) Proposed macro-model for the analysis of infilled frame structures. Bull N Z Soc Earthq Eng 40(2):69–77

D'Ayala D, Meslem A, Vamvatsikos D, Porter K, Rossetto T, Crowley H et al (2015) Guidelines for analytical vulnerability assessment—low/mid-rise. GEM Tech Rep 08:162. https://doi.org/10.13117/GEM.VULN-MOD.TR2014.12

Dolšek M, Fajfar P (2004) Inelastic spectra for infilled reinforced concrete frames. Earthq Eng Struct Dyn 33(15):1395–1416. https://doi.org/10.1002/eqe.410

Dolšek M, Fajfar P (2005) Simplified non-linear seismic analysis of infilled reinforced concrete frames. Earthq Eng Struct Dyn 34(1):49–66. https://doi.org/10.1002/eqe.411
Fajfar P, Dolšek M (2012) A practice-oriented estimation of the failure probability of building structures. Earthq Eng Struct Dyn 41(3):531–547. https://doi.org/10.1002/eqe.1143
FEMA (2000) FEMA 356: pretandardand commentary for the seismic rehabilitation of buildings. FEMA, Washington, DC
FEMA (2005) FEMA 440: improvement of nonlinear static seismic analysis procedures. FEMA, Washington, DC
FEMA (2009) FEMA P695: quantification of building seismic performance factors. FEMA, Washington, DC
FEMA (2012) FEMA P-58-1: seismic performance assessment of buildings: volume 1—methodology, vol 1. FEMA, Washington, DC
Furtado A, Rodrigues H, Arêde A, Varum H (2016) Experimental evaluation of out-of-plane capacity of masonry infill walls. Eng Struct 111:48–63. https://doi.org/10.1016/j.engstruct.2015.12.013
Hak S, Morandi P, Magenes G, Sullivan TJ (2012) Damage control for clay masonry infills in the design of RC frame structures. J Earthq Eng 16(Supp 1):1–35. https://doi.org/10.1080/13632469.2012.670575
Kazantzi AK, Vamvatsikos D (2018) The hysteretic energy as a performance measure in analytical studies. Earthq Spectra. https://doi.org/10.1193/112816eqs207m
McKenna F, Scott MH, Fenves GL (2010) Nonlinear finite-element analysis software architecture using object composition. J Comput Civ Eng 24(1):95–107. https://doi.org/10.1061/(ASCE)CP.1943-5487.0000002
Miranda E (2000) Inelastic displacement ratios for structures on firm sites. J Struct Eng 126(10):1150–1159. https://doi.org/10.1061/(ASCE)0733-9445(2000)126:10(1150)
Newmark NM, Hall JF (1982) Earthquake spectra design. University of California, Berkeley
O'Reilly GJ, Monteiro R (2019) Probabilistic models for structures with bilinear demand-intensity relationships. Earthq Eng Struct Dyn 48(2):253–268. https://doi.org/10.1002/eqe.3135.
O'Reilly GJ, Sullivan TJ (2017) Modeling techniques for the seismic assessment of the existing Italian RC frame structures. J Earthq Eng. https://doi.org/10.1080/13632469.2017.1360224
O'Reilly GJ, Sullivan TJ (2018a) Probabilistic seismic assessment and retrofit considerations for Italian RC frame buildings. Bull Earthq Eng 16(3):1447–1485. https://doi.org/10.1007/s10518-017-0257-9
O'Reilly GJ, Sullivan TJ (2018b) Quantification of modelling uncertainty in existing Italian RC frames. Earthq Eng Struct Dyn 47(4):1054–1074. https://doi.org/10.1002/eqe.3005
O'Reilly GJ, Kohrangi M, Bazzurro P, Monteiro R (2018a) Intensity measures for the collapse assessment of infilled RC frames. In: 16th European conference on earthquake engineering, Thessaloniki
O'Reilly GJ, Sullivan TJ, Monteiro R (2018b) On the seismic assessment and retrofit of infilled RC frames structures. In: 16th European conference on earthquake engineering, Thessaloniki
O'Reilly GJ, Perrone D, Fox M, Monteiro R, Filiatrault A (2018c) Seismic assessment and loss estimation of existing school buildings in Italy. Eng Struct 168:142–162. https://doi.org/10.1016/j.engstruct.2018.04.056
O'Reilly GJ, Perrone D, Fox M, Monteiro R, Filiatrault A, Lanese I et al (2019) System identification and seismic assessment modeling implications for Italian school buildings. J Perform Constr Facil 33(1):04018089. https://doi.org/10.1061/(ASCE)CF.1943-5509.0001237
Pasca M, Liberatore L, Masiani R (2017) Reliability of analytical models for the prediction of out-of-plane capacity of masonry infills. Struct Eng Mech 64(6):765–781. https://doi.org/10.12989/sem.2017.64.6.765
Pinto PE, Franchin P (2014) Existing buildings: the new Italian provisions for probabilistic seismic assessment. In: Ansal A (ed) Perspectives on European earthquake engineering and seismology. Springer, Berlin. https://doi.org/10.1007/978-3-319-07118-3_3
Ricci P, Di Domenico M, Verderame GM (2018) Experimental assessment of the in-plane/out-of-plane interaction in unreinforced masonry infill walls. Eng Struct 173:960–978. https://doi.org/10.1016/j.engstruct.2018.07.033
Vamvatsikos D (2002) Seismic performance, capacity and reliability of structures as seen through incremental dynamic analysis. PhD thesis, Stanford University, Stanford
Vamvatsikos D (2013) Derivation of new SAC/FEMA performance evaluation solutions with second-order hazard approximation. Earthq Eng Struct Dyn 42(8):1171–1188. https://doi.org/10.1002/eqe.2265
Vamvatsikos D, Cornell CA (2002) Incremental dynamic analysis. Earthq Eng Struct Dyn 31(3):491–514. https://doi.org/10.1002/eqe.141
Vamvatsikos D, Cornell CA (2005) Direct estimation of seismic demand and capacity of multidegree-of-freedom systems through incremental dynamic analysis of single degree of freedom approximation. J Struct Eng 131(4):589–599. https://doi.org/10.1061/(ASCE)0733-9445(2005)131:4(589)

Veletsos AS, Newmark NM (1960). Effect of inelastic behavior on the response of simple systems to earthquake motions. In; Proceedings of the 3rd world conference on earthquake engineering

Vidic T, Fajfar P, Fischinger M (1994) Consistent inelastic design spectra: strength and displacement. Earthq Eng Struct Dyn 23(5):507–521. https://doi.org/10.1002/eqe.4290230504

Villar-Vega M, Silva V, Crowley H, Yepes C, Tarque N, Acevedo AB et al (2017) Development of a fragility model for the residential building stock in South America. Earthq Spectra 33(2):581–604. https://doi.org/10.1193/010716EQS005M

Vorechovsky M, Novak D (2003) Statistical correlation in stratified sampling. In: Der Kiureghian A, Madant S, Pestana J (eds) ICAPS 9 proceedings of international conference on applications of statistics and probability in civil engineering. Millpress, Rotterdam